Structural Basis of m^{7}GpppG Binding to Poly(A)-Specific Ribonuclease

Mousheng Wu,[1,2,5,6] Per Nilsson,[3,5] Niklas Henriksson,[3,5] Anna Niedzwiecka,[4] Meng Kiat Lim,[1] Zhihong Cheng,[1] Kyriakos Kokkoris,[3] Anders Virtanen,[3] and Haiwei Song[1,2,*]

[1]Institute of Molecular and Cell Biology, Proteos, Singapore
[2]Department of Biological Sciences, National University of Singapore, Singapore
[3]Department of Cell and Molecular Biology, Uppsala University, Uppsala, Sweden
[4]Institute of Physics, Polish Academy of Sciences, and Institute of Experimental Physics, Warsaw University, Warsaw, Poland
[5]These three authors contribute equally to this work.
[6]Present address: Center for Membrane Biology, Department of Biochemistry and Molecular Biology,
University of Texas-Houston Medical School, Houston, TX 77030, USA.
*Correspondence: haiwei@imcb.a-star.edu.sg
DOI 10.1016/j.str.2008.11.012

SUMMARY

Poly(A)-specific ribonuclease (PARN) is a homodimeric, processive, and cap-interacting 3′ exoribonuclease that efficiently degrades eukaryotic mRNA poly(A) tails. The crystal structure of a C-terminally truncated PARN in complex with m^{7}GpppG reveals that, in one subunit, m^{7}GpppG binds to a cavity formed by the RRM domain and the nuclease domain, whereas in the other subunit, it binds almost exclusively to the RRM domain. Importantly, our structural and competition data show that the cap-binding site overlaps with the active site in the nuclease domain. Mutational analysis demonstrates that residues involved in m^{7}G recognition are crucial for cap-stimulated deadenylation activity, and those involved in both cap and poly(A) binding are important for catalysis. A modeled PARN, which shows that the RRM domain from one subunit and the R3H domain from the other subunit enclose the active site, provides a structural foundation for further studies to elucidate the mechanism of PARN-mediated deadenylation.
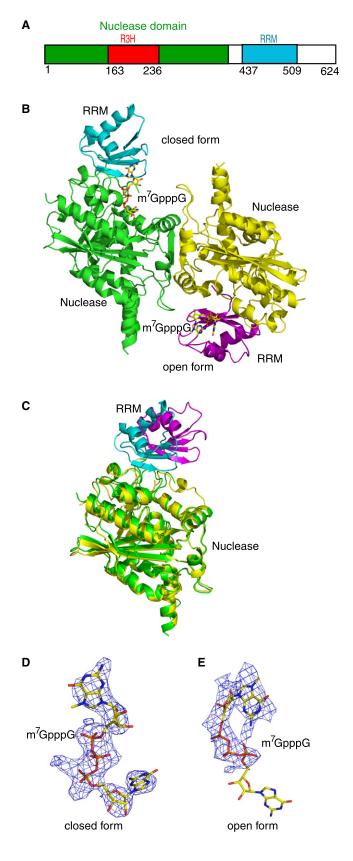
INTRODUCTION

The cap structure and the poly(A) tail are characteristic features of eukaryotic mRNA and are important for controlling RNA processing, transport, translation, and stability (reviewed in Garneau et al., 2007; Meyer et al., 2004; Parker and Song, 2004; and Shatkin and Manley, 2000). Many cap-binding proteins, such as the nuclear (CBP20) or the cytoplasmic (eIF4E) cap-binding proteins (Izaurralde et al., 1994; Sonenberg et al., 1978; von der Haar et al., 2004), and poly(A)-binding proteins, such as the nuclear or cytoplasmic poly(A)-binding proteins (PABP), are involved in these processes (reviewed in Kuhn and Wahle, 2004). Furthermore, both structures and, especially, the poly(A) tail are crucial for proper regulation of mRNA decay. Two general mRNA decay pathways have been identified, both of which are initiated by deadenylation of the mRNA poly(A) tail by deadenylases (reviewed in Garneau et al., 2007; Meyer et al., 2004; and Parker and Song, 2004). In the 5′→3′ mRNA decay pathway, the mRNA 5′ cap structure is removed by decapping enzymes when a substantial part of the poly(A) tail has been degraded. After this decapping event, the 5′→3′ Xrn1 exonuclease will degrade the remaining part of mRNA starting at the 5′ end of the mRNA. In the 3′→5′ mRNA decay pathway, the cytoplasmic exosome complex will continue to degrade the mRNA body in the 3′→5′ direction after the mRNA poly(A) tail has been removed by the deadenylation event.

In mammalian cells, poly(A)-specific ribonuclease (PARN) is one of the known deadenylases responsible for mRNA deadenylation (Åström et al., 1991; Körner and Wahle, 1997; Körner et al., 1998; Martinez et al., 2000). Biochemical studies have shown that PARN is an mRNA cap-interacting protein (Dehlin et al., 2000; Gao et al., 2000; Martinez et al., 2001). The binding of the mRNA 5′ cap stimulates the catalytic activity of PARN purified from mammalian cells (Dehlin et al., 2000; Gao et al., 2000; Martinez et al., 2000) and enhances the processivity of PARN action (Martinez et al., 2001). PARN belongs to the RNase D superfamily of nucleases and harbors high specificity toward single-stranded poly(A) (Martinez et al., 2000). It is a metal ion-dependent, highly processive, and multidomain exonuclease composed of the nuclease domain, the R3H domain, and the RNA recognition motif (RRM) (Figure 1A). The nuclease domain contains the catalytic site and is responsible for the cleavage of the poly(A) tail, whereas the R3H domain has been implicated in poly(A) binding, although its exact role is still not clear (Martinez et al., 2001; Nilsson et al., 2007; Ren et al., 2002; Wu et al., 2005). Our previous structural work on the N-terminal domain of human PARN (hPARN), containing the nuclease and R3H domains, demonstrated that a homodimeric form of PARN is the structural and functional unit (Wu et al., 2005).

Biochemical and mutational studies of the hPARN RRM showed that the RRM by itself binds the cap and also contributes to poly(A)-specificity and that the cap- and poly(A)-binding sites on the RRM are both functionally and structurally separated from each other (Nilsson et al., 2007). One tryptophan (W475 in human) within the RRM has been identified as an essential residue required for cap binding. Consistent with this finding,

Figure 1. The Structure of the mPARNt-m⁷GpppG Complex

(A) Domain organization of mPARN showing the nuclease domain (green), the R3H domain (red), and the RRM domain (cyan).

(B) A ribbon diagram of the mPARNt-m⁷GpppG complex. The nuclease domains in the closed and open forms are colored in green and yellow, respectively. The RRM domains in the closed and open forms are colored in cyan and purple, respectively. The m⁷GpppG molecules are shown in stick model.

(C) Superimposition of the closed and open forms of mPARNt. The nuclease domains are colored as in panel B. The RRM domains in the closed and open forms are colored in cyan and purple, respectively.

(D and E) 3.0Å simulated annealing (SA) omit maps contoured at 2σ covering m⁷GpppG in the closed and open forms, respectively.

the NMR and crystal structures of the RRM domain of PARN in complex with the cap analog revealed that the m^7G base of the cap analog stacks with the aromatic side chain of W468 in mice, corresponding to W475 in humans (Monecke et al., 2008; Nagata et al., 2008). However, the molecular mechanism underlying the cap-stimulated deadenylation activity and how cap recognition and poly(A) cleavage are coordinated to each other remain elusive.

To understand the molecular basis of cap recognition by PARN and how this process increases its enzymatic processivity, we have determined the crystal structure of a mouse PARN (mPARN) polypeptide containing the nuclease, R3H, and RRM domains in complex with the cap analog, m^7GpppG, at a resolution of 3.0 Å. The structure reveals a novel cap-binding mode that is distinct from other cap-binding proteins. Structural and mutational analyses showed that the RRM confers the cap recognition specificity with the nuclease domain, providing additional binding affinity. We conclude that the cap-binding and active sites partially overlap both structurally and functionally in the nuclease domain.

RESULTS

Structure Determination

A C-terminally truncated mPARN (residues 1–510, designated mPARNt) containing the nuclease, the R3H, and the RRM domains was cloned and expressed as a His-tag fusion protein. To facilitate protein crystallization, the flexible His-tag region at the N terminus was removed by PreScission protease. The selenomethione (SeMet)-substituted mPARNt was cocrystallized with the m^7GpppG cap analog. The structure of mPARNt in complex with m^7GpppG was determined at a resolution of 3.0 Å by a combination of SeMet SAD and the molecular replacement using the coordinates of apo-hPARNn (PDB code: 2A1R) and the NMR structure of mouse RRM domain (1WHV). There are two mPARNt molecules in the asymmetric unit with each molecule binding to one cap analog. The final model was refined to working and R free factor of 29.8% and 33.3%, respectively (see Experimental Procedures and Table 1). Five regions (residues 37–44, 149–249, 365–367, 393–401, and 504–510) in molecule A and four regions in molecule B (residues 145–250, 358–369, 392–404, and 506–510) are disordered.

Overall Structure

mPARNt forms a homodimer in the structure of the mPARNt-m^7GpppG complex via the nuclease domain, with each subunit

Table 1. Data Collection and Refinement Statistics

Data collection	
Space group	$P2_12_12_1$
Unit cell dimension	
a/b/c (Å)	58.01/128.35/176.84
$\alpha/\beta/\gamma$ (°)	90.00/90.00/90.00
Resolution range (Å)	50−3.0
Completeness (%)	96 (96)
Unique reflections (N)	29,592
Redundancy	6.9 (5.5)
R_{merge} (%)[a]	10.1 (32.7)
I/σ	4.5 (2.3)
Refinement	
Resolution (Å)	20−3.0
Used reflections (N)	24,512
Total atoms (N)	6310
Protein atoms	6126
Nucleotide atoms	104
Water molecules	80
R_{work} (%)[b]	29.8
R_{free} (%)[c]	33.3
r.m.s deviation from ideal values	
Bond distance (Å)	0.013
Bond angle (°)	1.533
Ramchandran plot	
Most favored region	85.5%
Allowed region	14.2%
Generously allowed region	0.3%
Disallowed region	0%

Values in parentheses indicate the specific values in the highest resolution shell (3.2−3.0 Å).

[a] $R_{merge} = \sum |I_j - <I>| / \sum I_j$, where I_j is the intensity of an individual reflection, and $<I>$ is the average intensity of that reflection.

[b] $R_{work} = \sum ||F_o| - |F_c|| / \sum |F_c|$, where F_o denotes the observed structure factor amplitude, and F_c denotes the structure factor amplitude calculated from the model.

[c] R_{free} is as for R_{work} but calculated with 5.0% of randomly chosen reflections omitted from the refinement.

binding to one cap analog (Figure 1B). The dimerized nuclease domain is structurally identical to that in our previous hPARN nuclease domain structure (PDB code: 2A1R) (Wu et al., 2005). Although the electron density map clearly showed some features of the R3H domain in the apo-hPARN structure (Wu et al., 2005), the quality of the electron density is not good enough to allow us to build any residues in the R3H domain with confidence. Given this fact, the R3H domains in both subunits in the mPARNt-m^{7}GpppG complex are assumed to be disordered.

The RRM domain is composed of a four-stranded antiparallel β sheet and two α helices packed against the β sheet and is connected to the nuclease domain by a hinge region consisting of residues 429–439 (Figure 1B). Surprisingly, the two subunits of mPARNt in the mPARNt-m^{7}GpppG complex adopt very different conformations. Superposition of the nuclease domains showed that the orientation of the RRM domains differ by 30° in the

two subunits (Figure 1C). This difference in the orientations of the RRM domains with respect to the nuclease domains leads to markedly different cap-binding modes in both subunits. In one subunit (referred to as closed form), m^{7}GpppG is located in the cavity formed by the RRM and the nuclease domain, and has well-defined electron density, whereas in the other subunit (referred to as open form), only one guanosine residue (m^{7}G) of m^{7}GpppG that interacts with the RRM domain is well ordered (Figures 1D and 1E).
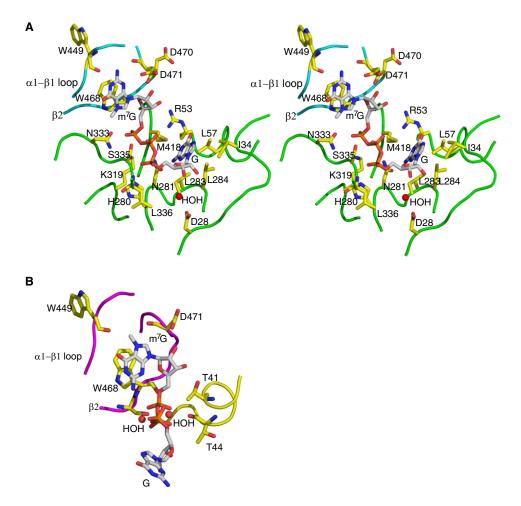
The Cap-Binding Site Is Formed by Both the RRM and Nuclease Domains

The 7-methyl guanosine group and the following guanosine group cannot be unambiguously differentiated in the electron density map of the mPARNt-m^{7}GpppG complex. However, there is a strong electron density facing to W468 in the mPARNt-m^{7}GpppG complex (Figures 1D and 1E). Moreover, a previous study showed that the RRM of hPARN by itself specifically interacted with the two cap analogs, m^{7}GTP and m^{7}GpppG, and that the W475 residue of hPARN (corresponding to W468 of mPARN; see Figure S1 available online) was critical for RRM-mediated cap analog binding (Nilsson et al., 2007). Thus, we fitted a model of m^{7}GpppG into the electron density in each subunit, with W468 stacking against the m^{7}G group. The correctness of this fitting is confirmed by the most recently determined structures of the RRM domain of PARN in complex, with the cap analog showing that the m^{7}G base stacks with W468 in mouse or W475 in human (Monecke et al., 2008; Nagata et al., 2008).

In the mPARNt-m^{7}GpppG complex, both the RRM and nuclease domains contribute to cap binding, with the nuclease domain involved in more-extensive interactions with the cap in the closed form than in the open form (Figure 2). In both forms, the m^{7}G recognition is conferred by residues from β2 and the α1-β1 loop of the RRM domain (Figure 2 and Figure S1). Specifically, the indole group of W468 in the RRM stacks against the m^{7}G base with a distance of 3.4Å in a coplanar orientation. Additionally, the carbonyl groups of W449 and D471 in the closed form make contacts with the N1 and N2 of the m^{7}G, respectively.

Our previous mutational study of the hPARN RRM showed that alanine substitutions of W475 and W456 in the RRM affected cap binding to different extent (Nilsson et al., 2007). It is likely that the severe effect of the W475A mutation was due to an interruption of the stacking interaction between this tryptophan residue and the 7-methyl guanine moiety of the cap. Mutation of W456 (corresponding to W449 in mice; Figure S1) to an alanine perturbed slightly the cap-binding property of hPARN. In the mPARNt-m^{7}GpppG complex, W449, F445, L454, Y497, and L457 form a hydrophobic core that stabilizes the RRM core structure (data not shown). A mutation of W449 would most likely distort the main-chain conformation of the α1-β1 loop, leading to the reduced cap-binding ability. The complex structure enables us to attribute the functional character to W475 (W468 in mice) and the structural role of W456 (W449 in mice) upon cap binding.

Previous studies showed that full-length hPARN binds m^{7}GpppG ∼2-fold better than m^{7}GTP (Nilsson et al., 2007). The binding affinity of the hPARN RRM domain to m^{7}GpppG or m^{7}GTP was about 7-fold lower than its binding affinity to the full-length protein, implying that other parts or domains of

Figure 2. The m⁷GpppG-Binding Site

(A) Stereo diagram of the mPARNt-m⁷GpppG interface in the closed form.

(B) The mPARNt-m⁷GpppG interface in the open form. Residues involved in the interaction and m⁷GpppG are shown in stick models. The color coding for mPARNt is as in Figure 1B.

PARN contributed to m⁷GpppG or m⁷GTP binding, although the RRM contributed primarily. In agreement with these biochemical results, our structure showed that the nuclease domain is also involved in cap binding (Figure 2).

In the closed form (Figure 2A), the 7-methylguanosine nucleoside assumes the *anti* conformation. Residues I34, L57, L283, L284, and M418 and the methyl group of R53 form a hydrophobic pocket for the first transcribed guanosine nucleotide. Of these residues, L284 and M418 clamp the guanosine and thus contribute significantly to the recognition of the first transcribed nucleotide of mRNA. The OD1 group of D28 interacts indirectly with the second ribose group via a water molecule. N281 makes multiple van der Waals contacts with O5 and O4 of the second ribose and N2 and N3 of the guanine base. In addition, the hydroxyl group of S335 contacts the second phosphate group. The NZ group of K319 contacts both the second and third phosphate groups. Furthermore, the third phosphate group makes multiple contacts with K319, H280, one water molecule, and the amino group of L336.

In the open form (Figure 2B), the 7-methylguanine moiety is still stacked with the W468 indol ring, but the m⁷G nucleoside adopts
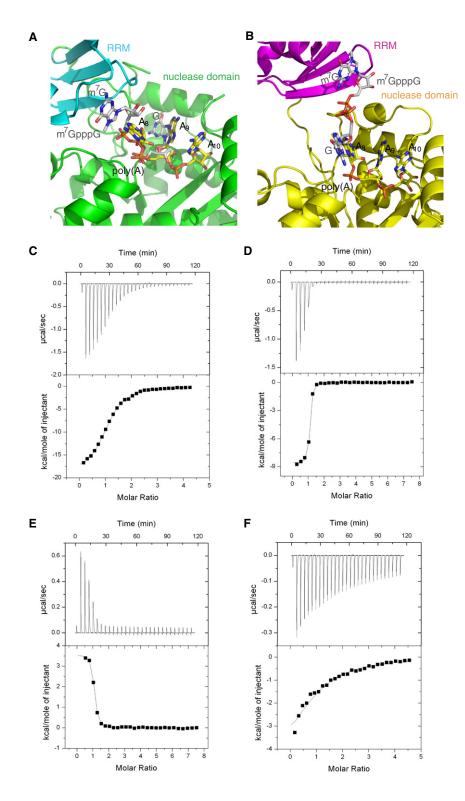
the *syn* conformation. Most of the noncovalent contacts stabilizing the phosphate bridge and the second nucleoside are lost. Only the D471 carboxylate and T41 make direct contacts with the first ribose and the first phosphate group of the cap, respectively, whereas T44 contacts the first phosphate group via a water molecule.

It should be noted that residues involved in the cap recognition (i.e., D28, I34, R53, L57, H280, N281, L283, L284, K319, N333, S335, L336, M418, R419, W449, W468, D470, and D471) are highly conserved in PARN family proteins, thereby underscoring their functional importance (Figure 2 and Figure S1). Taken together, these observations suggest that the nuclease domain provides additional binding affinity for cap recognition, particularly in the closed form.

The Cap-Binding Site of PARN Overlaps with the Active Site in the Nuclease Domain

The observations that some residues (i.e., D28 and I34) that have previously been shown to be critical for catalysis of hPARN are involved in cap binding (Figure 2A) imply that the cap-binding and active sites of PARN must overlap to some extent.

Figure 3. Poly(A) and m^7GpppG Compete with Each Other for Binding to PARN

(A and B) Superimposition of the bound A_3 in the hPARNn-poly(A) complex with the m^7GpppG molecule in the closed form (A) and in the open form (B). Color coding for mPARNt is as in Figure 1B. A_3 and m^7GpppG are shown in stick models with carbon atoms colored in yellow and gray, respectively.

(C) ITC titration of m^7GpppG into mPARNt.

(D) ITC titration of A_{10} into mPARNt.

(E) ITC titration of A_{10} into mPARNt in the presence of 2.5-fold excess of m^7GpppG.

(F) ITC titration of m^7GpppG into mPARNt in the presence of 2.5-fold excess of A_{10}. The upper panels show the experimental data, and the lower panels show the integrated heats for each injection together with the single-site model curves fitted to them.

the A8 and A9 bases, respectively, in the hPARNn-poly(A) complex, suggesting that residues involved in the cap binding may be important for catalytic activity of PARN as well. While in the open form, only the disordered G base overlaps to a minor extent with the adenine base A8 (Figure 3B), which was also poorly ordered in the structure of the hPARNn-poly(A) complex (Wu et al., 2005). These results suggest that, in the closed form, binding of m^7GpppG and poly(A) tail is mutually exclusive in a single PARN subunit, whereas the open form allows both cap and poly(A) tail binding simultaneously.

To examine whether m^7GpppG and poly(A) compete with each other for binding to PARN, isothermal titration calorimetry assays were performed. Titration of m^7GpppG into mPARNt showed that m^7GpppG binds to mPARNt with K_D of 2.1 μM at a molar ratio of ∼1.0 (Figure 3C and Table 2), suggesting that two cap analogs bind to one mPARNt dimer. This finding is consistent with the two cap-binding sites observed in the structure. Ten-mer oligo(A) (A_{10}) binds to mPARNt with nanomolar affinity (K_D = 0.06 μM; Figure 3D and Table 2) at a molar ratio of ∼1.0, suggesting that two A_{10} molecules bind to one PARN dimer. The tight binding of A_{10} to PARN can probably be attributed

Consistent with this notion, superposition of the mPARNt-m^7GpppG complex in the closed form with the hPARNn-poly(A) complex (Wu et al., 2005) showed that the bound m^7GpppG in the mPARNt-m^7GpppG complex overlaps substantially with the bound poly(A) in the hPARNn-poly(A) complex (Figure 3A). The phosphate linkage and the G base of m^7GpppG colocalize with

to the high-affinity binding of A_{10} to the canonical RNA-binding site on the RRM domain (Nilsson et al., 2007) and the binding of the 3′ end of A_{10} to the catalytic site in the nuclease domain (Wu et al., 2005). ITC competition assays showed that the binding of A_{10} to mPARNt was reduced by 3-fold in the presence of m^7GpppG (apparent dissociation constant [K_D^{app}] = 0.17 μM;

Table 2. Summary of Isothermal Titration Calorimetry Measurements

Protein in ITC cell	Ligand in syringe	K_D, µM	ΔH, kcal/mol	$T \Delta S$, kcal/mol	n
mPARNt	m⁷GpppG	2.1 ± 0.07	−19.3 ± 0.17	−11.7	1.08 ± 0.01
mPARNt	A_{10}	0.06 ± 0.005	−8.6 ± 0.05	1.02	1.01 ± 0.004
mPARNt + 2.5x m⁷GpppG	A_{10}	0.17 ± 0.01[a]	3.57 ± 0.03[a]	12.6[a]	0.99 ± 0.004
mPARNt + 2.5x A_{10}	m⁷GpppG	10.6 ± 1.2[a]	−5.22 ± 0.22[a]	1.41[a]	1.0[b]

[a] The apparent values of the dissociation constants and the resultant thermodynamic parameters, determined in the competition assay using a single-site model.
[b] Fixed value.

Figure 3E and Table 2), whereas the binding of m⁷GpppG to mPARNt was reduced by 12-fold (K_D^{app} = 10.6 µM; Figure 3F and Table 2) in the presence of A_{10}. Both interactions of mPARNt with the cap and A_{10} are enthalpy favorable, and the molar enthalpy change for the cap binding is twice more negative than that for A_{10}. Strikingly, titration of mPARNt with A_{10} after previous saturation of the protein by the cap analog leads to a positive enthalpy change. The observed sign inversion of ΔH suggests that most of the previously bound cap molecules are expulsed from the same or closely neighboring binding site by A_{10} as a result of much higher affinity of the latter. Taken together, these results strongly support the overlapped binding sites of cap and poly(A) observed in the structure and suggest that these overlapped binding sites are functionally relevant.

Functional Analysis of the Cap-Binding Site
To further characterize the cap-binding site and to investigate whether we could identify amino acids that play dual functional roles in both cap-binding and hydrolytic activity of PARN, we performed a site-directed mutational and functional analysis of hPARN (Table S1). For this analysis, we specifically targeted amino acid residues whose side chains were predicted from the mPARNt-m⁷GpppG complex to play a role in cap structure recognition and binding.

First we determined, by using fluorescence spectroscopy, the equilibrium dissociation constants (K_D) for the hPARN-m⁷GTP and hPARN-m⁷GpppG interactions (Table 3 and Figure S2). The shape of the titration curves for hPARN corresponds to a typical binding isotherm describing one type of binding site (Eftink, 1997), in accordance with what was observed by the ITC (Figure 3C). The hPARN-cap affinity is too weak to determine the stoichiometry directly from the numerical analysis of the fluorescence data (Niedzwiecka et al., 2007), but the crystal structure and the ITC results suggest that two cap molecules can bind to the PARN dimer concurrently (Figures 1B and 3C). The question is how the structural differences are reflected by the binding energetics. As we can see from Table 3, the dissociation constant for the dinucleotide cap analog is only less than 2-fold lower than that for the mononucleotide. In terms of the free energy of binding, the K_D values correspond to $\Delta G°$ of −8.11 and −7.77 kcal/mol, respectively. The difference is not significant, although the first transcribed nucleoside forms a network of noncovalent contacts with the protein (Figure 2A). By analogy, the affinity of the cap-binding site in the closed conformation, where both cap nucleotides are bound, will be only slightly stronger than the affinity of the open conformation. Hence, the two structurally different cap-binding sites can show similar energetic behavior, being indistinguishable in the titration assays.

In addition to the previously identified cap-binding-defective mutants, hPARN(W456A) and hPARN(W475A) (Nilsson et al., 2007), we identified another mutant polypeptide, hPARN(N288A), that was severely defective in binding both cap analogs and seven mutant polypeptides—hPARN(D28A), hPARN(I34A), hPARN(L291A), hPARN(K326A), hPARN(N340A), hPARN(S342A), and hPARN(R426A)—that were affected in binding to at least one of the cap analogs.

Next, we investigated the catalytic performance of the mutant hPARN polypeptides using three different kinds of RNA substrates—A_3, A_{20}, and noncapped L3(A_{30}). The A_3 substrate primarily probes the hydrolytic activity and poly(A)-binding property of the PARN active site, and the A_{20} substrate will rank the mutant polypeptides, because this substrate examines both hydrolytic activity in the active site and poly(A) binding within and outside the active site, whereas the L3(A_{30}) substrate will provide information regarding the catalytic efficiency when a substrate resembling noncapped mRNA substrates is used. Furthermore, the catalytic efficiency of PARN activity can accurately be quantified when the noncapped L3(A_{30}) substrate is used, because it is possible to follow and quantify the release

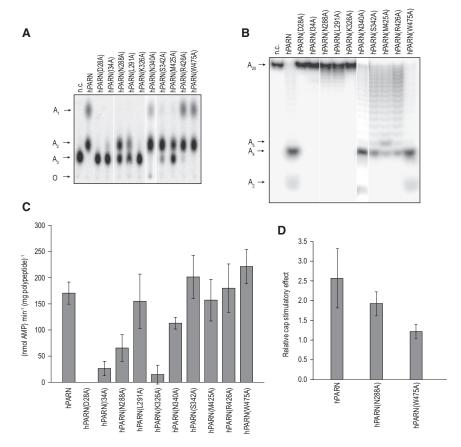**Table 3. Summary of hPARN-Cap Analog Equilibrium Dissociation Constants**

hPARN polypeptide[a]	$K_D ± \Delta K_D$ (µM)[b]	
	m⁷GTP	m⁷GpppG
PARN[c]	1.59 ± 0.11	0.90 ± 0.02
PARN(D28A)	2.71 ± 0.18	1.03 ± 0.05
PARN(I34A)	6.8 ± 0.7	3.05 ± 0.14
PARN(N288A)	>1000	>1000
PARN(L291A)	9.8 ± 1.0	1.32 ± 0.15
PARN(K326A)	2.36 ± 0.16	1.83 ± 0.19
PARN(N340A)	2.34 ± 0.08	0.88 ± 0.06
PARN(S342A)	1.9 ± 0.4	2.4 ± 0.6
PARN(M425A)	1.7 ± 0.13	0.96 ± 0.04
PARN(R426A)	3.7 ± 0.4	3.1 ± 0.3
PARN(W456A)[c]	5.6 ± 1.4	6.4 ± 0.8
PARN(W475A)[c]	>1000	>1000

Determined by intrinsic protein fluorescence quenching in 20 mM HEPES-KOH (pH 7), 100 mM KCl, 1.5 mM MgCl₂, 0.2 mM EDTA, 0.5 mM DTT, at 20°C.
[a] PARN mutants were generated by site-directed mutagenesis.
[b] Listed values are weighed averages ± experimental errors resulting from at least three independent titration series.
[c] Data from Nilsson et al., 2007.

A

B

C

D

Figure 4. Residues Involved in Cap Binding Are Important for PARN-Mediated Deadenylation

(A) 50 nM of hPARN or mutant hPARN polypeptide, as indicated, was incubated with 1 μM 5′-end ^{32}P-labeled A_3 substrate. Reaction products, A_2 and A_1, were separated by TLC, and the resulting fluorogram is shown. The hydrolytic activity of each polypeptide was investigated during at least three independent experiments. Representative TLC patterns are shown.

(B) 10 nM of hPARN or mutant hPARN polypeptide, as indicated, were incubated with 25 nM 5′-end ^{32}P-labeled A_{20} substrate. Reaction products were separated by denaturing 25% polyacrylamide gel electrophoresis, and the resulting fluorogram is shown. The positions of reaction products are as indicated. The hydrolytic activity of each polypeptide was investigated during at least three independent experiments. Representative electrophoretic fractionation patterns are shown.

(C) 10 nM hPARN or mutant hPARN polypeptide, as indicated, were incubated with 50 nM noncapped L3(A_{30}) substrate, radioactively labeled in its poly(A) tail. Released AMP products were fractionated by TLC. The amount of released AMP was quantified, and the resulting reaction rates—nmol AMP/(min*mg polypeptide)—based on at least three independent experiments, were calculated. Error bars represent 95% confidence intervals.

(D) hPARN or mutant hPARN polypeptide, as indicated, was incubated with 10 nM of m^{7}GpppG-capped or noncapped L3(A_{30}) substrate for 10 min in 30°C under phosphate buffer conditions (see Experimental Procedures). Released AMP products were fractionated by TLC (Figure S3). The cap-stimulatory effect was measured by calculating the ratio of the released amount of AMP from a reaction where hPARN or mutant hPARN polypeptide was incubated with a m^{7}GpppG-capped L3(A_{30}) substrate over the amount of released AMP from a reaction where hPARN or mutant hPARN polypeptide was incubated with a noncapped L3(A_{30}) substrate. Each bar represent mean values of ratios using 2, 4, 8, and 16 nM hPARN or mutant hPARN polypeptide from at least three independent experiments. Error bars represent 95% confidence intervals.
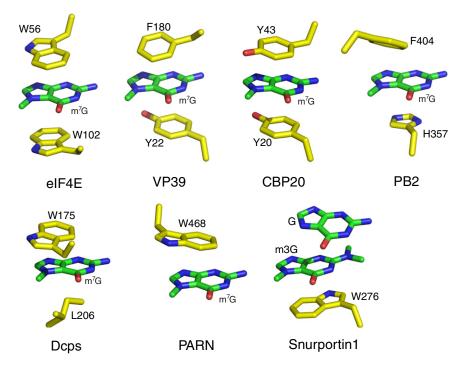
of the AMP product (Åström et al., 1991). The results from this analysis are summarized in Figures 4A–4C. Three classes of mutant hPARN polypeptides were identified: (1) a hydrolytically inactive or severely defective group including hPARN(D28A), hPARN(I34A), and hPARN(K326A); (2) a hydrolytically active group including hPARN(N288A), hPARN(L291A), hPARN(N340A), hPARN(S342A), hPARN(M425A), and hPARN(R426A), which revealed deficiencies when some of the substrates were used; and (3) one hydrolytically nondefective mutant polypeptide, hPARN(W475A). The catalytic performance of some of these mutant polypeptides—hPARN(D28A), hPARN(I34A), hPARN(K326A) and hPARN(W475A)—have been investigated earlier, and the current study is in keeping with those studies (Ren et al., 2004; Ren et al., 2002; Wu et al., 2005).

Earlier studies (Balatsos et al., 2006; Nilsson et al., 2007) have revealed that the cap-stimulatory effect on PARN cannot be recovered when recombinant hPARN purified from bacteria is used. However, we have recently established a phosphate-buffered in vitro deadenylation system wherein a 2.5-fold cap-stimulatory effect can be recovered when bacterially expressed hPARN is used (see Experimental Procedures, Figure 4D, and Figure S3). The magnitude of this stimulatory effect resembles the 3-fold effect that was observed when we used native PARN purified from calf thymus (Martinez et al., 2001). Having

established this new in vitro system, we investigated whether any of the two cap-binding-deficient and hydrolytically active mutants—hPARN(N288A) and hPARN(W475A)—were affected in cap stimulation (Figure S3). The results are summarized in Figure 4D and show that hPARN(W475A) did not reveal any cap-stimulatory effect, whereas the hPARN(N288A) mutant was slightly affected.

In conclusion, nine of the tested mutant polypeptides revealed either major or minor deficiencies in their deadenylation properties, suggesting that the targeted amino acid residues are required for proper performance of PARN deadenylation activity. Significantly, at least two of the mutant polypeptides—hPARN(I34A) and hPARN(N288A)—were clearly defective in both cap binding and deadenylation activities. Furthermore, mutations of residues N288, L291A, S342A, and M425A involved in the phosphate linkage and the G base recognition (Figure 2A) showed defects when converting A_2 to A_1 (Figure 4A). Finally, we have established in vitro deadenylation conditions wherein a cap-stimulatory effect, to a level corresponding to native PARN, can be recovered when bacterially produced recombinant hPARN is used and have identified at least one hydrolytically active mutant polypeptide, hPARN(W475A), that is deficient in both cap binding and the cap-stimulatory effect. Taken together, these results suggest that tryptophan residue 475 participates in both cap binding

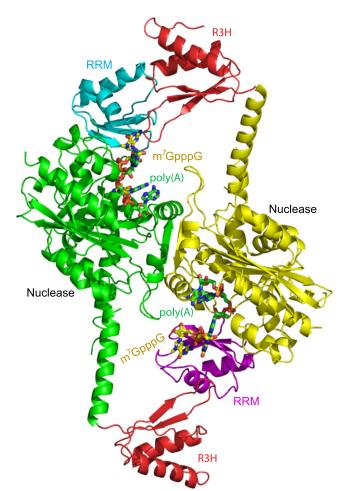**Figure 5. Comparisons of the m⁷G-Binding Modes in eIF4E, VP39, CBP20, PB2, Dcps, Snurportin1, and PARN**

The guanosine bases are colored in green stick models, and the residues involved in stacking interactions with the guanosine base are colored in yellow sticks and labeled.

is the only known example that exploits one-sided stacking to stabilize the m⁷G moiety and keeps an open space at the other side of its aromatic ring. The less efficient one-sided stacking in PARN is supported by a large network of other noncovalent contacts, especially those stabilizing the phosphate linkage and surrounding the first transcribed nucleoside. It was shown that PARN discriminated the 7-methylated 5′ terminus versus the nonmethylated one in the enzymatic assays when we used PARN purified from calf thymus (Martinez et al., 2001; Martinez et al., 2000); hence, the

and cap stimulation and that the cap-binding site overlaps to some extent, both structurally and functionally, with the active site of PARN at the nuclease domain.

DISCUSSION

Crystal structures of eIF4E (Marcotrigiano et al., 1997), the vaccinia virus protein Vp39 (Hodel et al., 1998), CBP20-CBP80 complex (Mazza et al., 2001), the scavenger mRNA decapping enzyme (DcpS) (Chen et al., 2005; Gu et al., 2004), and the nuclear import adaptor snurportin1 (Strasser et al., 2005) in complex with cap analogs have been determined. A comparison of these protein-cap complex structures has revealed a shared mechanism for cap structure recognition (Figure 5). This conserved mechanism is based on π-π or cation-π stacking interaction between aromatic residues of the protein and the methylated guanine moiety of the cap to discriminate a methylated guanine base from an unmethylated guanine (Hu et al., 2003; Niedzwiecka et al., 2002). In eIF4E, CBP20, and VP39, the 7-methyl guanosine moiety is sandwiched by two aromatic residues from these proteins, whereas in DcpS, it is sandwiched by W175 and L206 (Figure 5). Most recently, the crystal structure of the central domain of influenza virus polymerase subunit PB2 in complex with m⁷GTP showed that the m⁷G base is sandwiched between F404 and H357 (Guilligay et al., 2008) (Figure 5). In the snurportin1-m₃²,²,⁷GpppG complex, the cap analog is self-stacked, providing the third stacking plane (Strasser et al., 2005). Our structure showed that only one aromatic residue, W468, stacks against the 7-methyl guanosine base (Figure 5).

To sum up, we have identified a novel mode of 7-methylguanosine cap recognition by PARN. Although the stacking interaction, salt bridges, direct and water-mediated hydrogen bonds, and van der Waals contacts that contribute to the cap recognition by PARN are common among cap-binding proteins, PARN

one-sided stacking provided by the platform made up by the indol ring of W468 (W475 in human) seems to be the minimal, necessary, and sufficient condition for specificity toward the 7-methylguanosine cap structure.

The RNA recognition motif (RRM) is one of the most abundant protein domains in eukaryotes and participates in many biological processes, such as RNA editing, RNA splicing, RNA export, translational regulation, and RNA degradation (Maris et al., 2005). To date, there are more than 30 structures of RRMs determined by NMR or X-ray crystallography. The RRMs share a common αβ fold structure with a βαββαβ topology. The β strands form an antiparallel β sheet and are packed against by two α helices. Previous extensive biochemical studies on the RRM of hPARN showed that this RRM binds both the cap structure and poly(A) (Nilsson et al., 2007). In keeping with these observations, our current structure indicates that PARN utilizes the α1-β1 loop and β2 in the RRM domain to recognize the m⁷G moiety and that the nuclease domain contacts the rest of the cap molecule. The canonical RNA-binding site on the RRM domain β face is still available for poly(A) binding.

To date, we have determined three structures of PARN—hPARNn (residues 1–430) in native form, hPARNn (residues 1–430) in complex with poly(A), and the mPARNt-m⁷GpppG complex—and have shown that PARN functions as a homodimer. Given that we have not succeeded in observing all three functional domains of PARN simultaneously in a single structure, we reconstructed a homodimeric model of PARN by superimposing these three structures together given that the position of the disordered R3H domain in the mPARNt-m7GpppG complex is likely to be the same as in the apo-hPARNn (see above) (Wu et al., 2005) (Figure 6). This model shows that the RRM domain from one subunit, together with the R3H domain from the other subunit, forms a circular structure that encloses the active site. Consistent with this view, deletion mutation

Figure 6. Model of Homodimeric PARN Containing All Three Functional Domains

Color coding for the RRM and nuclease domains is as in Figure 1. The R3H domain is colored in red. m^{7}GpppG and poly(A) are shown in stick models with carbon atoms colored in yellow and green, respectively.

and thermal stability studies showed that the R3H domain cross-talked with the RRM domain to stabilize hPARN (Liu et al., 2007). In this circular structure, the RRM domain may act in conjunction with the R3H domain to increase the processivity of PARN, although the underlying mechanism remains elusive.

We have characterized the cap-binding site of PARN through a combined structural and functional analysis. Most importantly, we show that the cap-binding and active sites of PARN partially overlap both structurally and functionally within the nuclease domain. This is a major surprise because earlier biochemical studies clearly indicated that the two sites were structurally and functionally separate from each other (Martinez et al., 2001). This apparent discrepancy may be resolved by a putative mechanism wherein the cap and poly(A) bind individually to two subunits of PARN (Figure 6). The observations that the homodimeric PARN in the mPARNt-m7GpppG complex contains two structurally distinct cap-binding sites are similar to those observed in the Dcps structure (Gu et al., 2004). Although the dramatically asymmetric cap-binding sites in Dcps suggested an elegant autoregulatory mechanism to control scavenger

mRNA decapping, the functional implications of the distinct-cap binding sites in PARN do not seem very clear. The conformational changes that are induced upon cap binding might be tightly coupled to the stimulatory effect of the 5′ cap on the poly(A) tail hydrolysis. However, the molecular basis of how the cap binding is coordinated with the poly(A) binding to stimulate hydrolysis remains to be elucidated.

In summary, the mPARNt-m^{7}GpppG complex structure presented here reveals a novel cap-binding mode. Both the RRM and the nuclease domains are involved in cap binding, with the RRM recognizing the m^{7}G base and the nuclease domain providing additional binding affinity for the rest of the cap molecule. Importantly, our structural and mutational data demonstrated that the cap-binding site and the active site overlap each other both structurally and functionally. Superposition of all the PARN structures we have solved so far allows us to reconstruct a homodimeric model of PARN. This model will be essential for further studies when elucidating molecular mechanisms behind PARN action, including its catalytic activity, high specificity for poly(A), processivity, and the molecular details behind the cap stimulatory effect on PARN.

EXPERIMENTAL PROCEDURES

Molecular Cloning

mPARNt was amplified from mouse full-length PARN cDNA (RZPD, Germany) with a forward primer containing PreScission protease cutting site. The fragment was cloned into a pET28a vector.

Site-Directed Mutagenesis

hPARN mutants were generated from pE$_{33}$PARN (Ren et al., 2002) using Quick-Change Site-Directed Mutagenesis kit (Stratagene) following the protocol from the manufacturer. The mutations were introduced by using primers named as the corresponding mutation and with sequences listed in Table S2. All mutations were confirmed by DNA sequencing.

Protein Expression and Purification

mPARNt was expressed in *Escherichia coli* strain BL-21 STAR (Stratagene). Cells were induced with 0.1 mM IPTG when OD$_{600nm}$ reached 0.6 and were further incubated at 18°C overnight. Selenomethione-substituted protein was expressed by growing cells in a minimum media containing 20 mg/L L-seleno-methione (Sigma). The cells were harvested and resuspended in a lysis buffer (20 mM Tris [pH 8.0], 500 mM NaCl, and 2 mM benzamidine) containing 1 mg/ml lysozyme. The cells were lysed using sonication and were centrifuged at 18,000 g for 1 hr. The supernatant was loaded onto a Talon Affinity Resin (Clontech) column and was washed with at least 10 column volumes of the lysis buffer containing 20 mM imidazole. The mPARNt protein was eluted with the lysis buffer containing 200 mM imidazole. The His tag was removed by the PreScission protease (Amersham) at 4°C overnight, and the target protein was further purified using MonoQ and Superdex-200 columns (Amersham). The protein was concentrated to about 10 mg/ml for crystallization.

Recombinant hPARN(D28A), hPARN(I34A), hPARN(N288A), hPARN(L291A), hPARN(K326A), hPARN(N340A), hPARN(S342A), hPARN(M425A), hPARN(R426A), and hPARN(W475A) were expressed from *E. coli* strain BL21(DE3), as described elsewhere (Nilsson and Virtanen, 2006). Soluble recombinant polypeptides were purified using Talon Metal Affinity Resin (Clontech). The amount of protein was measured using a BioRad protein assay kit, and the purity was analyzed by gel electrophoresis (SDS-PAGE) followed by silver or coomassie staining.

Preparation of RNA Substrates

A$_3$ and A$_{20}$ RNA substrates were purchased from Dharmacon Research. Before usage, the substrates were deprotected according to the instructions from the manufacturer. A$_3$ or A$_{20}$ (10 pmol) was 5′-labeled with 20 pmol

[γ-^{32}P]-ATP (GE Healthcare, cat nr AA0068) using T4 polynucleotide kinase (USB, cat nr 70031Z), and the reaction was incubated in 37°C for 45 min. The labeled nucleotides were resolved by 25% polyacrylamide gel, bands cut out and eluted over night in water. The final concentrations of labeled oligo(A) were 2.5–25 nM. m^{7}GpppG capped or noncapped L3(A$_{30}$) was prepared by in vitro transcription, as described elsewhere (Nilsson et al., 2007).

Crystallization, Data Collection, and Structure Determination

m^{7}GpppG cap analog was added to the protein solution to a final concentration of 1 mM. The crystals of mPARNt with m^{7}GpppG were grown in a buffer containing 6–10% PEG6000, 100 mM MES [pH6.0], and 10 mM betaine by use of the hanging-drop method. The crystals were cryo-protected in the above crystallization condition with 35% Ethylene glycol and were frozen in liquid nitrogen. A SeMet SAD data set was collected at ID14-4 in ESRF (Grenoble, France) and was processed with MOSFLM and CCP4 (CCP4, 1994). The crystal belongs to space group P2$_1$2$_1$2$_1$, with two molecules in the asymmetric unit. The structure of mPARNt in complex m^{7}GpppG was determined with a combination of SeMet SAD and the molecular replacement method using Phaser (McCoy et al., 2005). Our previous structure of the nuclease domain of hPARNn (pdb code: 2A1R) and the NMR model of mouse RRM (pdb code: 1WHV) were used as search models in the molecular replacement. The phases generated by SeMet SAD phasing using SHARP (De la fortelle and Bricogne, 1997) were combined with those from the model to calculate the initial electron density map. Model rebuilding was carried out with Coot (Emsley and Cowtan, 2004). The model was refined by CNS (Brunger et al., 1998) and refmac5 (Murshudov et al., 1997). All data statistics are shown in Table 1.

Fluorescence Spectroscopy

Titrations were performed essentially as described elsewhere (Niedzwiecka et al., 2007). The cap analogs were a kind gift of Edward Darżynkiewicz, University of Warsaw. The protein samples were centrifuged for 10 min at 12,000 rpm at 4°C. hPARN and mutants thereof were used at 0.06–0.5 μM per monomer, in 20 mM HEPES-KOH (pH 7), 100 mM KCl, 1.5 mM MgCl$_2$, 0.5 mM DTT, and 0.2 mM EDTA. Aliquots of 1 μl of increasing concentrations (10 μM to 2 mM) of m^{7}GTP or m^{7}GpppG were injected manually to 1400 μl of protein solution. Fluorescence measurements were run on Fluorolog-3 Spectrofluorometer (Horiba Jobin Yvon), at 20.0°C in a thermostated quartz semi-micro cuvette (Hellma), at an excitation and emission wavelengths of 280 and 320 nm (slit 1 and 10 nm), respectively. Fluorescence changes were monitored continuously with the integration time of 30 s and the gap of 30 s for adding the ligand, with slow magnetic stirring. During the gap, the excitation slit was shut off to avoid photobleaching of the sample. The signal was normalized by the reference photodiode current. Regressions were performed by means of a nonlinear, least-squares method, using PRISM 3.02 (GraphPad Software, USA). The final K$_D$ values were calculated as weighted averages from at least three independent titration series.

PARN Deadenylation Assay

hPARN or hPARN mutant (50 nM) was incubated with 1 μM A$_3$. Conditions for the reaction were 25 mM HEPES (pH 7.0), 100 mM NaCl, 0.1 μg/μl BSA, and 2 mM MgCl$_2$. The reactions (final volume, 10 μl) were incubated at 30°C for 10 min and were stopped by the addition of 2 μl of 0.5 M EDTA. Released AMP products were separated from the reactions by one-dimensional TLC by spotting 1 μl of the reaction on a polyethyleneimine cellulose F plate (Merck, 5579) and using 0.5 M LiCl as solvent. The plate was dried, exposed, and scanned by a 400S PhosphorImager (Molecular Dynamics).

hPARN or hPARN mutant (10 nM) was incubated with 25 nM A$_{20}$. Reaction conditions were as described above. The reacted RNA was separated by 25% polyacrylamide (19:1 acrylamide:bis-acrylamide). The gel was exposed and scanned by a 400S PhosphorImager (Molecular Dynamics).

hPARN or hPARN mutants (1–128 nM) were incubated with 10–50 nM m^{7}GpppG capped or noncapped L3(A$_{30}$), as described above or when indicated, in 50 mM KH$_2$PO$_4$/K$_2$HPO$_4$ (pH 7.0), 100 mM NaCl, 0.1 μg/μl BSA, and 2 mM MgCl$_2$. Released AMP products were separated from the reactions by one-dimensional TLC by spotting 1 μl of the reaction on a polyethyleneimine cellulose F plate (Merck, 5579) and using 0.4 M KH$_2$PO$_4$ (pH 3.5) (H$_3$PO$_4$) as solvent. The plate was dried, exposed, and scanned with a 400S PhosphorImager (Molecular Dynamics).

Isothermal Titration Calorimetry

The binding affinities of mPARNt to m^{7}GpppG and 10-mer poly(A) (A$_{10}$) were determined using a VP-ITC microcalorimeter (Microcal, Inc). Twenty-nine aliquots of 10 μl of 290 μM m^{7}GpppG or 480 μM A$_{10}$ in the syringe were titrated against 15 μM mPARNt (concentration calculated per PARN monomer) in the cell at 18°C in the buffer containing 100 mM KCl, 25 mM potassium phosphate (pH 7.5), 1 mM DTT, and 5 mM EDTA. In the case of competition assay, mPARNt was mixed with m^{7}GpppG or A$_{10}$ with molar ratio of 2.5:1 and was titrated by A$_{10}$ or m^{7}GpppG, respectively. The heat of dilution was measured by additional injections of ligand after saturation. The titration curves were analyzed using MicroCal Origin software. The K$_D$ and K$_D^{app}$ values were calculated using the equation for the single-site model, where K$_D$ = 1/ K$_a$.

ACCESSION NUMBERS

The coordinates and structure factors for the mPARNt-m^{7}GpppG complex have been deposited in the Protein Data Bank (accession number 3D45).

SUPPLEMENTAL DATA

Supplemental data include two tables and three figures and can be found with this article online at http://www.cell.com/structure/supplemental/S0969-2126(09)00029-X.

REFERENCES

Åström, J., Åström, A., and Virtanen, A. (1991). In vitro deadenylation of mammalian mRNA by a HeLa cell 3′ exonuclease. EMBO J. 10, 3067–3071.

Balatsos, N.A., Nilsson, P., Mazza, C., Cusack, S., and Virtanen, A. (2006). Inhibition of mRNA deadenylation by the nuclear cap binding complex (CBC). J. Biol. Chem. 281, 4517–4522.

Brunger, A.T., Adams, P.D., Clore, G.M., DeLano, W.L., Gros, P., Grosse-Kunstleve, R.W., Jiang, J.S., Kuszewski, J., Nilges, M., Pannu, N.S., et al. (1998). Crystallography & NMR system: A new software suite for macromolecular structure determination. Acta Crystallogr. D Biol. Crystallogr. 54, 905–921.

CCP4. (1994). The CCP4 suite: programs for protein crystallography. Acta Crystallogr. D Biol. Crystallogr. 50, 760–763.

Chen, N., Walsh, M.A., Liu, Y., Parker, R., and Song, H. (2005). Crystal structures of human DcpS in ligand-free and m7GDP-bound forms suggest a dynamic mechanism for scavenger mRNA decapping. J. Mol. Biol. 347, 707–718.

De la fortelle, E., and Bricogne, G. (1997). Maximum-likelihood heavy-atom parameter refinement for multiple isomorphous replacement and multiwavelength anomalous diffraction method. Methods Enzymol. 276, 472–494.

Dehlin, E., Wormington, M., Körner, C.G., and Wahle, E. (2000). Cap-dependent deadenylation of mRNA. EMBO J. 19, 1079–1086.

Eftink, M.R. (1997). Fluorescence methods for studying equilibrium macromolecule-ligand interactions. Methods Enzymol. 278, 221–257.

Emsley, P., and Cowtan, K. (2004). Coot: model-building tools for molecular graphics. Acta Crystallogr. D Biol. Crystallogr. 60, 2126–2132.

Gao, M., Fritz, D.T., Ford, L.P., and Wilusz, J. (2000). Interaction between a poly(A)-specific ribonuclease and the 5′ cap influences mRNA deadenylation rates in vitro. Mol. Cell *5*, 479–488.

Garneau, N.L., Wilusz, J., and Wilusz, C.J. (2007). The highways and byways of mRNA decay. Nat. Rev. Mol. Cell Biol. *8*, 113–126.

Gu, M., Fabrega, C., Liu, S.-W., Liu, H., Kiledjian, M., and Lima, C.D. (2004). Insights into the structure, mechanism, and regulation of scavenger mRNA decapping activity. Mol. Cell *14*, 67–80.

Guilligay, D., Tarendeau, F., Resa-Infante, P., Coloma, R., Crepin, T., Sehr, P., Lewis, J., Ruigrok, R.W., Ortin, J., Hart, D.J., and Cusack, S. (2008). The structural basis for cap binding by influenza virus polymerase subunit PB2. Nat. Struct. Mol. Biol. *15*, 500–506.

Hodel, A.E., Gershon, P.D., and Quiocho, F.A. (1998). Structural basis for sequence-nonspecific recognition of 5′-capped mRNA by a cap-modifying enzyme. Mol. Cell *1*, 443–447.

Hu, G., Tsai, A.L., and Quiocho, F.A. (2003). Insertion of an N7-methylguanine mRNA cap between two coplanar aromatic residues of a cap-binding protein is fast and selective for a positively charged cap. J. Biol. Chem. *278*, 51515–51520.

Izaurralde, E., Lewis, J., McGuigan, C., Jankowska, M., Darzynkiewicz, E., and Mattaj, I.W. (1994). A nuclear cap binding protein complex involved in pre-mRNA splicing. Cell *78*, 657–668.

Körner, C.G., and Wahle, E. (1997). Poly(A) tail shortening by a mammalian poly(A)-specific 3′-exoribonuclease. J. Biol. Chem. *272*, 10448–10456.

Körner, C.G., Wormington, M., Muckenthaler, M., Schneider, S., Dehlin, E., and Wahle, E. (1998). The deadenylating nuclease (DAN) is involved in poly(A) tail removal during the meiotic maturation of Xenopus oocytes. EMBO J. *17*, 5427–5437.

Kuhn, U., and Wahle, E. (2004). Structure and function of poly(A) binding proteins. Biochim. Biophys. Acta *1678*, 67–84.

Liu, W.F., Zhang, A., He, G.J., and Yan, Y.B. (2007). The R3H domain stabilizes poly(A)-specific ribonuclease by stabilizing the RRM domain. Biochem. Biophys. Res. Commun. *360*, 846–851.

Marcotrigiano, J., Gingras, A.-C., Sonenberg, N., and Burley, S.K. (1997). Cocrystal structure of the messenger RNA 5′ cap-binding protein (eIF4E) bound to 7-methyl-GDP. Cell *89*, 951–961.

Maris, C., Dominguez, C., and Allain, F.H. (2005). The RNA recognition motif, a plastic RNA-binding platform to regulate post-transcriptional gene expression. FEBS J. *272*, 2118–2131.

Martinez, J., Ren, Y.-G., Nilsson, P., Ehrenberg, M., and Virtanen, A. (2001). The mRNA cap structure stimulates rate of poly(A) removal and amplifies processivity of degradation. J. Biol. Chem. *276*, 27923–27929.

Martinez, J., Ren, Y.-G., Thuresson, A.-C., Hellman, U., Astrom, J., and Virtanen, A. (2000). A 54-kDa fragment of the poly(A)-specific ribonuclease is an oligomeric, processive, and cap-interacting poly(A)-specific 3′ exonuclease. J. Biol. Chem. *275*, 24222–24230.

Mazza, C., Ohno, M., Segref, A., Mattaj, I.W., and Cusack, S. (2001). Crystal structure of the human nuclear cap binding complex. Mol. Cell *8*, 383–396.

McCoy, A.J., Grosse-Kunstleve, R.W., Storoni, L.C., and Read, R.J. (2005). Likelihood-enhanced fast translation functions. Acta Crystallogr. D Biol. Crystallogr. *61*, 458–464.

Meyer, S., Temme, C., and Wahle, E. (2004). Messanger RNA turnover in eukaryotes: pathways and enzymes. Crit. Rev. Biochem. Mol. Biol. *39*, 197–216.

Monecke, T., Schell, S., Dickmanns, A., and Ficner, R. (2008). Crystal structure of the RRM domain of poly(A)-specific ribonuclease reveals a novel m(7)G-cap-binding mode. J. Mol. Biol. *382*, 827–834.

Murshudov, G.N., Vagin, A.A., and Dodson, E.J. (1997). Refinement of macro-molecular structures by the maximum-likelihood method. Acta Crystallogr. D Biol. Crystallogr. *53*, 240–255.

Nagata, T., Suzuki, S., Endo, R., Shirouzu, M., Terada, T., Inoue, M., Kigawa, T., Kobayashi, N., Guntert, P., Tanaka, A., et al. (2008). The RRM domain of poly(A)-specific ribonuclease has a noncanonical binding site for mRNA cap analog recognition. Nucleic Acids Res. *36*, 4754–4767.

Niedzwiecka, A., Marcotrigiano, J., Stepinski, J., Jankowska-Anyszka, M., Wyslouch-Cieszynska, A., Dadlez, M., Gingras, A.C., Mak, P., Darzynkiewicz, E., Sonenberg, N., et al. (2002). Biophysical studies of eIF4E cap-binding protein: recognition of mRNA 5′ cap structure and synthetic fragments of eIF4G and 4E-BP1 proteins. J. Mol. Biol. *319*, 615–635.

Niedzwiecka, A., Stepinski, J., Antosiewicz, J.M., Darzynkiewicz, E., and Stolarski, R. (2007). Biophysical Approach to Studies of Cap-eIF4E Interaction by Synthetic Cap Analogs. In Translation Initiation: Reconstituted Systems and Biophysical Methods, J. Lorsch, ed. (San Diego: Academic Press), pp. 209–245.

Nilsson, P., and Virtanen, A. (2006). Expression and purification of recombinant poly(A)-specific ribonuclease (PARN). Int. J. Biol. Macromol. *39*, 95–99.

Nilsson, P., Henriksson, N., Niedzwiecka, A., Balatsos, N.A.A., Kokkoris, K., Eriksson, J., and Virtanen, A. (2007). A multifunctional RNA recognition motif in poly(A)-specific ribonuclease with cap and poly(A) binding properties. J. Biol. Chem. *282*, 32902–32911.

Parker, R., and Song, H. (2004). The enzymes and control of eukaryotic mRNA turnover. Nat. Struct. Mol. Biol. *11*, 121–127.

Ren, Y.G., Martinez, J., and Virtanen, A. (2002). Identification of the active site of poly(A)-specific ribonuclease by site-directed mutagenesis and Fe(2+)-mediated cleavage. J. Biol. Chem. *277*, 5982–5987.

Ren, Y.G., Kirsebom, L.A., and Virtanen, A. (2004). Coordination of divalent metal ions in the active site of poly(A)-specific ribonuclease. J. Biol. Chem. *279*, 48702–48706.

Shatkin, A.J., and Manley, J.L. (2000). The ends of the affair: capping and poly-adenylation. Nat. Struct. Biol. *7*, 838–842.

Sonenberg, N., Morgan, M.A., Merrick, W.C., and Shatkin, A.J. (1978). A poly-peptide in eukaryotic initiation factors that crosslinks specifically to the 5′-terminal cap in mRNA. Proc. Natl. Acad. Sci. USA *75*, 4843–4847.

Strasser, A., Dickmanns, A., Luhrmann, R., and Ficner, R. (2005). Structural basis for m3G-cap-mediated nuclear import of spliceosomal UsnRNPs by snurportin1. EMBO J. *24*, 2235–2243.

von der Haar, T., Gross, J.D., Wagner, G., and McCarthy, J.E.G. (2004). The mRNA cap-binding protein eIF4E in post-transcriptional gene expression. Nat. Struct. Mol. Biol. *11*, 503–511.

Wu, M., Reuter, M., Lilie, H., Liu, Y., Wahle, E., and Song, H. (2005). Structural insight into poly(A) binding and catalytic mechanism of human PARN. EMBO J. *24*, 4082–4093.